T-Junction Loaded with Interdigital Capacitor for Differential Measurement of Permittivity

Pejman Mohammadi[1,2], Ali Mohammadi, Member, IEEE, and Ali Kara, Senior Member, IEEE

***Abstract*— The microwave sensors have been successfully used for permittivity measurement. These sensors suffer from limited sensitivity and environmental effects. This paper presents a novel T-junction highly sensitive microwave sensor for permittivity measurement of low loss solid materials. The proposed sensor operation principle is based on downshifting the transmission zero of the outputs of T-junction with the coupling of the material under test (MUT). The sensing section consist of an interdigital capacitor (IDC) located in between the lines of the T-junction. IDC is directly connected to output arms of T-junction so that it could disturb the outputs strongly. Any change in electric field concentration in IDC directly is transmitted to the outputs and is translated as TZ change. Design steps including T-junction and IDC effects on outputs are presented in details. The sensor operation principle is described through an equivalent circuit model which is validated by simulation and experimental results. Two outputs of the proposed sensor show the same electrical performances which allow differential operation mode. Hence, cross sensitivity due to environmental factors can be tolerated by the sensor. Measurement results of the fabricated prototype shows $112\ MHz$ frequency shift per unit permittivity change, and a normalized sensitivity of 3.9 %, which are larger than available similar sensors. The proposed sensor is implemented on a $22.22 \times 18.76 \times 1.6\ mm^3$ printed circuit board.**

***Index Terms*— T-junction, Interdigital capacitor, sensor, high sensitivity.**

I. INTRODUCTION

PERMITTIVITY is one of the main features for characterizing material reaction to the applied electric fields. Microwave sensors based on the response of Material Under Test (MUT) to electromagnetic fields have found many applications in industry, environmental pollution and biomedical systems [1-4]. These sensors offer high potential for real time characterizations of solid materials [5-8]. Wireless sensing [1] and high Q sensor [6] have been implemented using Split Ring Resonator (SRR) for permittivity detection. Microplastic detection in water and soil are explored using resonance microwave reflectometry, in which resonance frequencies shift as a function of the relative permittivity [2]. A microwave strain sensor [4] based on chip less tag reader shows high elongation range and high sensitivity response. In [8] a microstrip line sensor is used to determine the dielectric constant of solid material with a pair of electrically coupled resonator. However, only the materials permittivity in 2.5GHz are evaluated. Sensitivity, size and environmental effects on the sensor response have limited the performance of available microwave sensors. Sensitivity depends on the electrical field concentration. Different design techniques like SRRs, Complementary Split Ring Resonators (CSRRs), and meandered microstrip line are used to increase sensitivity. Loading different topologies of SRRs [5-7] and CSRRs [9-11] on host transmission lines changes the electric-field or magnetic-field distribution and generate transmission zeros (TZs) or transmission poles (TPs) in the frequency response. The sensitivity of these microwave sensors is highly dependent on SRRs or CSRRs shape, size and orientation [12-14]. Meandered microstrip line and interdigital structures have been used recently in microwave sensors to achieve higher sensitivity [15-17]. Capacitively-loaded periodic slow-wave transmission line for dielectric constant measurement is presented in [15]. The achieved sensitivity is higher than ordinary meandered line with similar dimensions. An ultra-sensitive microwave sensor with meander slot in CSRR in order to enhance the field confinement is reported [16]. The majority of the sensors reported previously suffer from cross-sensitivity to the environmental effects such as temperature and humidity. Differential sensors are known to have inherent robustness to the cross-sensitivity as they typically consist of two independent sensing elements for differential operation. In this class of sensors, the variations in the ambient factors are taken as a common mode input to the detection mechanism. A pair of meandered microstrip transmission lines for differential sensing with optimized sensitivity is implemented [17]. Microwave sensor in [18] is composed of a microstrip meandered line with T-shaped resonator and an interdigital structure. Interaction between interdigital structure and T-shaped resonator leads to increased electric field intensity, which translates higher sensitivity. With a folded microstrip line, loaded with an interdigital line and a stub, a microwave sensor with dual mode applications is realized in [19]. For permittivity and permeability measurements, inter-digital capacitor (IDC) based SRR and meandered line based SRR offer higher sensitivity

1- Pejman Mohammadi is with the Department of Electrical Engineering, Urmia Branch, Islamic Azad University, Urmia, Iran (e-mail: p.mohammadi@ iaurmia.ac.ir).
2- Pejman Mohammadi is with the Microwave and Antenna Research Center, Urmia Branch, Islamic Azad University, Urmia, Iran.
Ali Mohammadi is with Department of Electronic and Electrical Engineering, University of Bath (e-mail: a.mohammadi@bath.ac.uk).
Ali Kara is with the Department of Electrical and Electronics Engineering, Faculty of Engineering, Gazi University, Ankara 06570, Turkey (e-mail: akara@gazi.edu.tr).

[20]. In [21] a biosensor is made with a quarter wavelength stub for glucose monitoring. Stub is connected to a microstrip feed line in one end and to an IDC at the other end as sensing area. A microfluidic detector for characterization of aqueous solutions with, a planar folded quarter wavelength type resonator etched in the central conductor of a coplanar waveguide is reported in [22]. IDC implementation in Substrate Integrated Waveguide (SIW) results in negative-order-resonance operation and significant level of miniaturization for permittivity detection sensor [23]. Microwave patch resonator in [24] uses aperture coupling for humidity detection but the sensor response is easily changed by temperature and humidity. Therefore, the sensor must be calibrated for each measurement. Concentration of mixed nitrate and phosphate in water is measured with a microstrip line loaded with CSRR as reported in [25]. However, it requires a temperature system containing a controller (REX-C100), heater, thermocouple sensor and solid-state relay to control the temperature at test point. This leads to a complicated measurement setup.

This paper reports a new microwave sensor topology for permittivity measurement of low loss solid materials. As to the knowledge of the authors, this sensor is the first design published in the literature. The host of the sensor is a T-junction power divider with two equal outputs. Therefore, the sensor can be operating in differential mode for higher immunity against environmental effects. An IDC is etched in between the two outputs of the T-junction in order to confine the electric field, and to produce a capacitor-like characteristics. Subsequently, a TZ is measured at the outputs of the proposed structure. The operation principle is based on downshifting the TZ with changing permittivity of the MUT. The designed sensor targets high sensitivity, small size and robustness against environmental effects.

The paper is organized as follows: Section II presents design of T-junction power divider along with overall sensor structure. Equivalent circuit model, parametric analysis and sensitivity analysis are also given in this section. Section III presents experimental results and performance comparison with existing sensors reported in the literature. Finally, section IV draws key conclusions.

II. PROPOSED PERMITTIVITY SENSOR CONFIGURATION

The proposed sensor consists of a T-Junction power divider as a host and an IDC as a sensing transducer. IDC is embedded in between the two arms of the T-junction. The design procedure of the T-junction and the analysis of the IDC are overviewed in the following. The length and the width of IDC fingers are investigated for TZs changes. Electromagnetic simulations regarding the T-junction with and without the IDC demonstrate sensing capability of the sensor. Based on the simulation results, the electromagnetic (EM) model verifies the validity of the equivalent circuit model.

A. *T-junction Power Divider*

T-junction power divider is a three-port network that can be used for power division or power combining in transmission lines [26]. The host in the proposed sensor is a T-junction in the form of microstrip line as shown in Fig. 1(a). Two quarter wavelength transmission lines with characteristic impedance of $Z_s = \sqrt{2}Z_0$ are used to match the input microstrip line with characteristic impedance Z_0. Transmission line model shown in Fig.1(b) illustrates that the input port views two quarter wavelength lines arranged as two parallel loads. Then, the input port is

$$Y_{in} = Y_2 + Y_3 \tag{1}$$

where $Y_2 = Y_3 = 0.5Y_0$.

Y_2 and Y_3 are the input admittance from the junction toward the port 2 and the port 3, respectively. They are determined from load (Z_0) connected to the quarter wavelength (Z_s) lines. The fringing fields associated with the discontinuity at the junction leads to storing energy. They are accounted by negligible susceptance here.

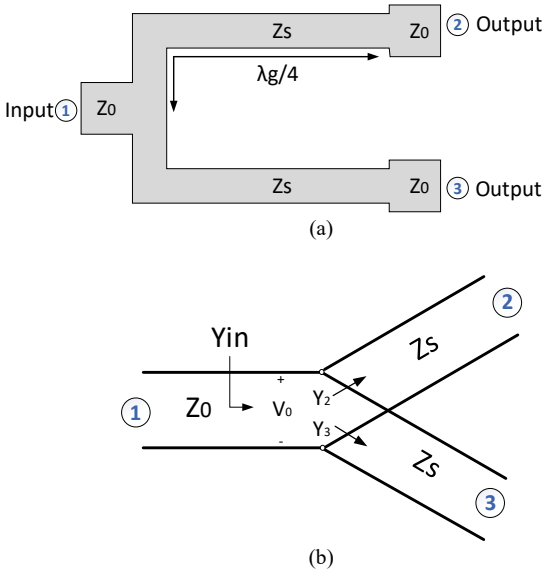

Fig. 1 T-junction (a) Layout (b) Transmission line model.

As the proposed T-junction is a symmetrical structure, its output ports receive equal power according to

$$P_i = \frac{1}{2} v_0^2 Y_i \tag{2}$$

where $i = 2,3$ and P_i denotes the output power at *i*-th port.

B. *Interdigital capacitor (IDC)*

The objective of the IDC is to provide the desired capacitance-like effect for the targeted frequency band. The capacitance occurs across the gaps and discontinuities

incorporated into the structure like open ends. Analysis and characterization of IDCs have been reported in [27]. Full-wave numerical solution by CST software is used for the IDC characterization in the proposed sensor. The capacitance increases as the gaps, or the distance between fingers, are decrease. The gap size, fingers' length and width are used in the IDC optimization to generate a notch in the desired band. The optimized parameters of the IDC and simulation results are provided in next section.

C. *Sensor Design*

The operational frequency of the T-junction is selected to satisfy operational frequency band of the overall sensor, i.e., the Industrial, Scientific and Medical (ISM) band. The simulation results of the S-Parameters for proposed T-junction and IDC are shown in Fig. 2 (a) and (b) respectively. The outputs (S31 and S21) receive equal-power, and the input is matched at the targeted band according to Fig. 2 (a). The EM simulation of the proposed IDC in Fig. 2 (b) shows that there is a notch in desired frequency band. The layout of the proposed sensor including the T-junction as host transmission line and the IDC as sensing area is shown in Fig. 3. The host has symmetrical configuration and IDC is positioned in between the output lines of the T-junction. Embedding the IDC within the T-junction generates a TZ (TZ_0=2.838GHz) in transfer functions (S21 and S31) as shown in Fig. 4. Hence, TZ_0 shifts down in response to permittivity increase of the solid MUTs placed on top of the sensor. The TZs of sensor together with MUTs are expected to be smaller than TZ_0 due to increase the permittivity. The operational band of the T-junction (f_0) is determined such that its 3dB outputs be positioned in the targeted frequency band (ISM). It should be noted that the length of the T-junction arms is dependent on the operation frequency. Therefore, the operation frequency could be adjusted with the length of the T-junction arms in accordance with permittivity of the MUT. The size of the IDC is optimized according to the desired responses. Hence, the size of the structure and the operational frequency band are dependent on two parameters. Therefore, the design process is focused on independent designs of the T-junction and the IDC with respect to the targeted operational frequency band.

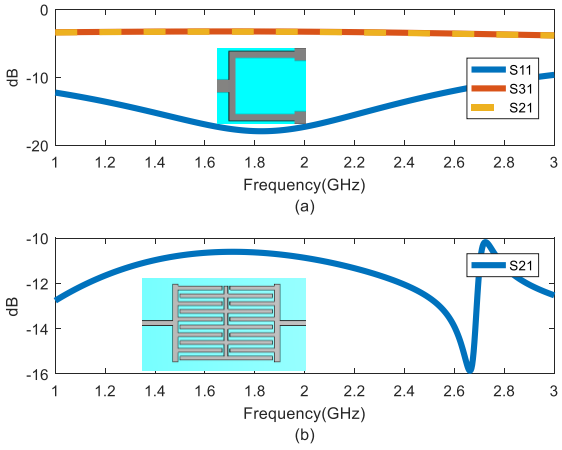

Fig. 2 The simulation results of (a) the proposed T-junction (b) the IDC.

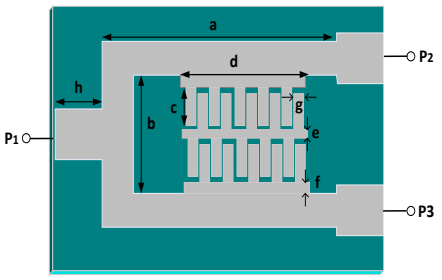

Fig. 3 Layout of the proposed sensor.

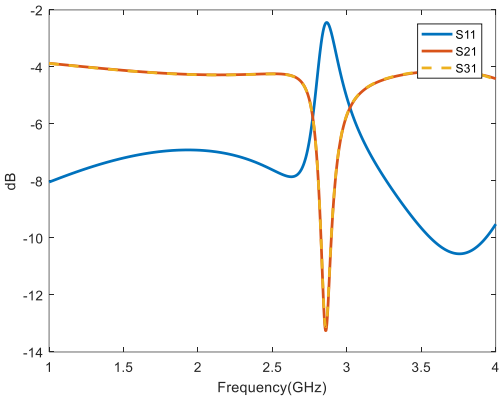

Fig. 4 The s-parameter simulation of the proposed sensor.

D. *Equivalent Circuit Model*

The equivalent circuit model in Fig. 5 (a) is extracted from EM simulation results for the proposed sensor of Fig.4. This includes three transmission lines to model the T-junction and two LC that model the IDC. As shown, the capacitance effect between the IDC and the ground is modeled with two capacitors in each arm. The length of transmission line output arms of the T-junction is slightly extended for the compensation of the inductive and capacitive effects. The capacitance arises through additional charge accumulation at the corners particularly at the outer point of the bend where electric fields concentrate. The inductive arises because of current flow interruption [28]. IDC is modeled with parallel connection of L_1 and C_1. Coupling components (inductances) between the arms P2 and P3 are included in the model. Also, the capacitive effects between the output arms and IDC fingers (not connected directly to output arms) are also modeled, as shown in Fig. 5 (c). Scattering parameters from EM simulation and circuit model of T-junction are compared in Fig. 5 (b). The EM and circuit model present similar responses. Fig. 5(c) shows the simulation results of EM and circuit model of the proposed sensor. The notch frequency of transmission coefficients is close to each other, which can be derived from [3]:

$$f_z = \frac{1}{2\pi\sqrt{L_1 C_1}} \tag{3}$$

This simple circuit model is valid for the operational frequency band frequencies. The circuit model parameters and sensor dimensions in Fig. 3 are given in TABLE I.

TABLE I
SENSOR DIMENSIONS and CIRCUIT MODEL PARAMETERS

a	b	c	d	E	f	g	$M(nH)$
16.26	14	5.8	10	0.5	0.7	0.5	0.001
$L_1(nH)$	$C_1(pF)$	$Z_1(\Omega)$	$Z_2(\Omega)$	θ_2	h	C(pF)	$C_2(pF)$
1.02	3.06	50	$50\sqrt{2}$	$\frac{\lambda_g}{4}$	3	0.10	10.5

Length in mm.

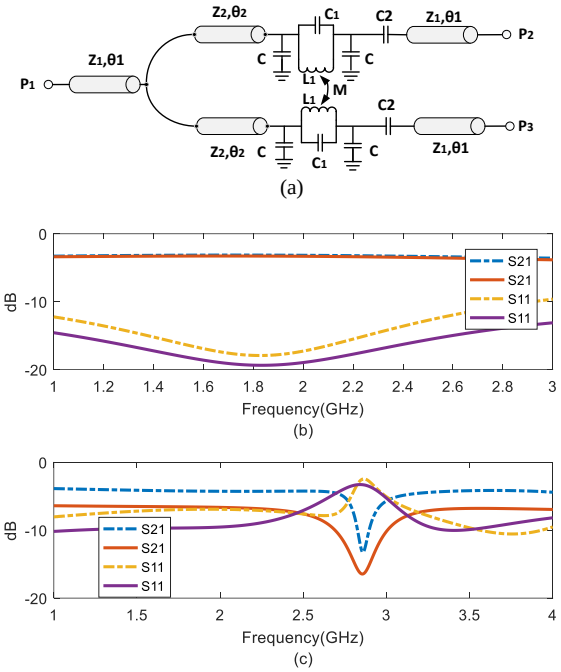

Fig. 5. (a) The equivalent circuit model (solid line), the simulation (dashed line) results of the (b) T-junction and (c) the proposed sensor.

E. Parametric Analysis

The design of the T-junction targets ISM band operation for the proposed sensor. Then, its dimensions are fixed. On the other hand, the IDC dimensions could be examined in parametric studies. The impact of the IDC fingers' length (c) and the fingers' width (g) on TZ of S21 is shown in Fig. 6 (a) and Fig. 6 (b) respectively. When c increases, the coupling between IDC fingers increases. However, reducing the gap between the fingers leads to an increase in the width of the fingers. These variations result in increasing the capacitive effects, that is, C_1. Hence, the TZ decreases according to (3). Minimum required sample size without significant performance degradation of the sensor is also investigated by simulating different sample widths and lengths. The variation of the sensor sensitivity, as per the notch frequency, with respect to the size of the sample is shown in Table II. As expected, the sensor sensitivity is proportional to the sample size as the electric field in the sensing area gets smaller as the sample size gets smaller. The minimum (or optimal) size of the sample would be around 100 mm^2.

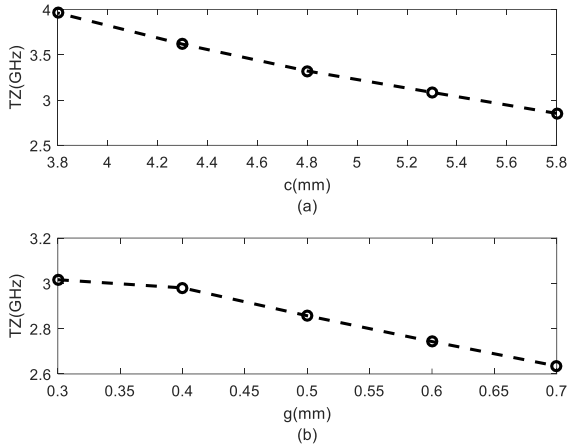

Fig. 6 Effect of (a) finger length (b) finger width of IDC on TZ of the proposed sensor.

TABLE II
SENSITIVITY FOR DIFFERENT SAMPLE SIZE

Sample Size (mm^2)	165	117	77	45	21
S%	4.3	3.86	2.6	1.3	0.25

F. Sensitivity analysis

The sensitivity of the proposed sensor has been discussed by running simulations in addition to theoretical analysis. MUT has been added on IDC in simulation environment. The size of example MUT is 15×11×2 mm^3. The permittivity of MUT has been swept from 1 to 10 incremented in steps of 1, and the TZ frequencies are recorded. In order to develop an explicit formula between permittivity and TZ polynomial, curve fitting model is derived in (4) [3].

$$f_{zi} = \mathrm{a}_i \times 10^{-4}\epsilon_r{}^3 + \mathrm{b}_i \times 10^{-2}\epsilon_r{}^2 + \mathrm{c}_i \times 10^{-1}\epsilon_r + d_i \qquad i = S, M \tag{4}$$

Polynomial coefficients are given in TABEL II.
Theoretical sensitivity is defined as the normalized variation of TZ frequency with respect to permittivity, could be derived from (5).

$$S = \frac{\partial f_z}{f_o \partial \epsilon_r} \times 100 \tag{5}$$

Where f_z is the TZ, f_o is the TZ of unloaded sensor and ϵ_r is the relative permittivity of the load. The TZs and simulation sensitivity for different permittivity values are shown in Fig. 8 (a) and Fig. 8 (b) respectively based on (4) and (5). Increasing the permittivity of the MUT samples, increase the capacitance and inductance of IDC (L_1 *and* C_1) in equivalent circuit model, which reduces the TZ frequency according to (3). Fig. 8 (b) shows that sensitivity decreases for larger permittivity values.

In our design, the MUT is considered to be lossless or low loss. However, the EM simulations with some degree of loss are also studied. The simulation results presented in Fig. 7 shows that magnitude of transmission coefficient is highly dependent on the dielectric loss. However, the TZ values do not vary significantly in response to dielectric loss changes.

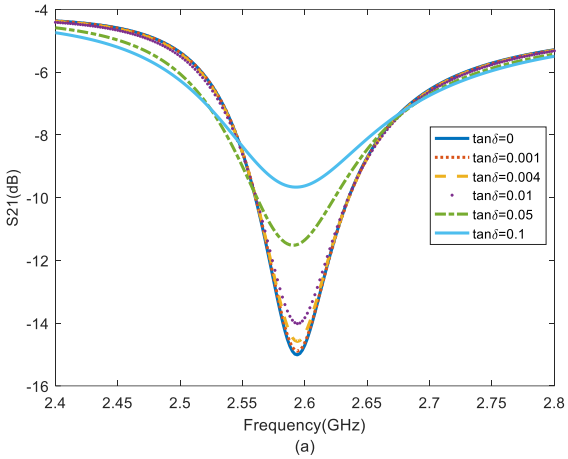

(a)

Fig. 7 s-parameter variation for different loss tangent values (lossy material with $\epsilon_r = 2$).

III. Experimental Results

A prototype sensor device has been developed on printed circuit board to validate the proposed sensing technique and to evaluate the developed model. Then measurements were conducted with different solid materials (MUTs). The measurements were repeated ten times and the average is taken to remove measurement errors.

A. *Measurement results*

The proposed sensor is designed on FR4 ($h = 1.6mm$, $tan\delta = 0.018$, $\varepsilon_r = 4.3$), with the operation frequency of $f_0 = 1.812\,GHz$. The width of 50 Ω microstrip lines and quarter wavelength lines are 3.1 mm and 1.66 mm corresponding to characteristic impedances. The fabricated sensor with measurement setup is shown in Fig. 8.

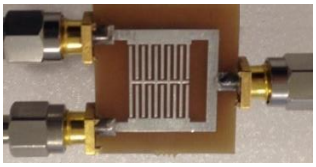
(a)

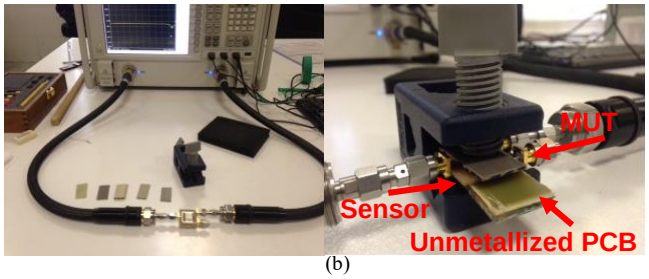

(b)

Fig. 8 (a) The fabricated sensor (b) Measurement set up.

Measurement set up comprises the proposed sensor, a clamp with plastic screw, unmetallized MUTs and a piece of unmetallized PCB. MUTs samples are located on top of the sensor and un-metallized PCB is placed under the sensor. The clamp fixes the MUT on the sensor with a screw to ensure consistent approach. Rectangular shaped test samples with a size of 15 × 20 mm^2 are cut from unmetallized microwave substrates. The size of the samples is adjusted as per the sensing area of the sensor. The thickness of the samples is slightly larger than 1.2 mm in order to remove the effects of the thickness on TZs of the proposed sensor.

The available test samples are RT Duroid 5870 ($\epsilon_r = 2.33$ $h = 1.575$mm), FR4 ($\epsilon_r = 4.3$ $h = 1.6$ mm), RT Duroid 6006 ($\epsilon_r = 6$ $h = 1.905$ mm), RT Duroid 6010 ($\epsilon_r = 10.22$ $h = 1.9$ mm).

TABLE III
POLYNOMIAL MODEL COEFFICIENTS

i	a_i	b_i	c_i	d_i
S	−9.199	2.417	−2.852	3.133
M	−5.491	1.698	−2.315	3.102

S: Simulation, M: Measurement

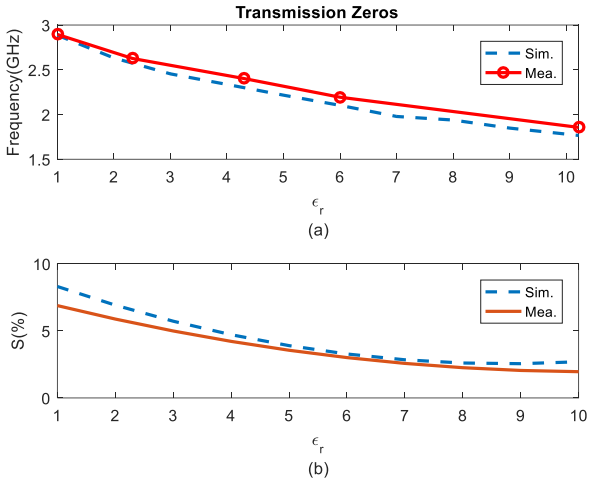

(a)
(b)

Fig. 9 (a) Measured and simulated TZs in terms of MUT permittivity (b) Measured and simulated sensitivity as a function of MUT permittivity.

TABLE IV
MEASUREMENT RESULTS FOR DIFFERENT SAMPLES

Sample	ϵ_r	TZs (GHz)
Bare	1	2.895
RT 5870	2.33	2.626
FR4	1.6	2.402
RT 6006	6	2.193
RT 6010	10.22	1.865

Samples of available substrates are examined on the sensor and measured TZs are recorded as shown in TABLE IV. The dependency between permittivity of the test samples and associated TZs could be extracted with polynomial curve fitting

model in (4) with coefficients in TABLE III. The TZ frequencies obtained from simulations and measurements for different permittivity values are illustrated in Fig. 9 (a). The experimental sensitivity is obtained using (5). The measured sensitivity seems to be consistent with the simulations, especially, mid-range of MUT permittivity. The normalized sensitivity for a sensor could be achieved from (6), where f_{o1} and f_{o2} are upper and lower frequencies respectively, in the targeted band. From the simulations, $f_o = f_{o1} = 2.848$ GHz and $f_{o2} = 1.771$ GHz are obtained which means 1.077 GHz frequency shift within the permittivity range. The normalized theoretical sensitivity value is 4.1 % according to (6).

$$S_n = \frac{1}{f_o}\frac{\Delta f}{\Delta \epsilon_r} \times 100 \quad (6)$$

$$\Delta f = f_{o2} - f_{o1} \quad (7)$$

On the other hand, in experiment $f_{01} = 2.895\ GHz$, $f_{02} = 1.865\ GHz$ leads to a frequency shift of $\Delta f = 1.03\ GHz$ (TABLE IV). This corresponds to a normalized experimental sensitivity of 3.9 %, shows 112 MHz frequency shift per unit permittivity change, which is larger than available sensors. The measurement setup shown in Fig.10(a) is used to measure the s-parameters of the differential outputs (port 2 and 3) while the input port (port 1) is matched. Fig.10(b) presents the s-parameters between the differential ports, where a notch and a transmission pole are visible. The measurement results for bare sensor show 3 MHz difference between the notches of S22 and S33. Moreover, we observed the effects of the positioning of materials over the sensor. The horizontal positioning effects result in larger changes in resonant frequency of S22 and S33 compared with the vertical positioning effects, which was negligible. In order to characterize the extreme frequency shifts caused by position of the material, we shifted the material up to 2mm in horizontal direction, which results in 5 MHz change in the resonant frequency of S22 and S33. Beyond 2mm shifting, one of the outputs disappears. Therefore, in order to obtain maximum accuracy this sensors require samples with at least 1.4 mm thickness on top of IDC (best location) with the size of 140 mm2. A set of experiments are conducted with available samples to measure the shifting in the notch. Then, the measurement sensitivity is found to be 4.3% based on (6). On the other hand, the effect of the sample thickness is also studied by increasing the sample thickness and simulating the shift in the notch. Fig.10(c) shows the variation of the notch with various sample thickness values. The minimum thickness where the notch does not respond is around 1.4mm. The thickness of the targeted samples listed in Table IV seems to be adequate. Therefore, the proposed sensor achieves the targeted accuracy.

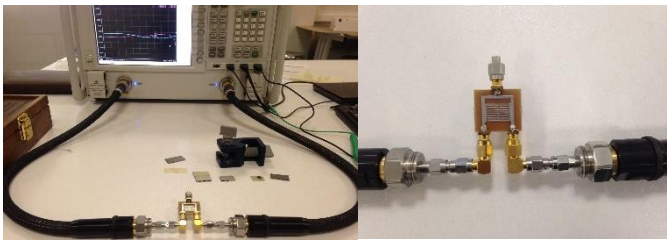

(a)

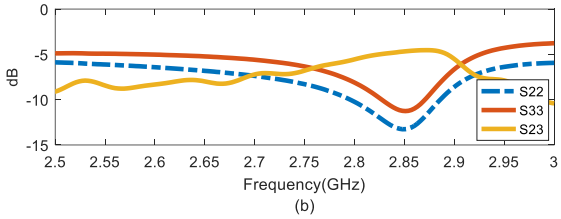

(b)

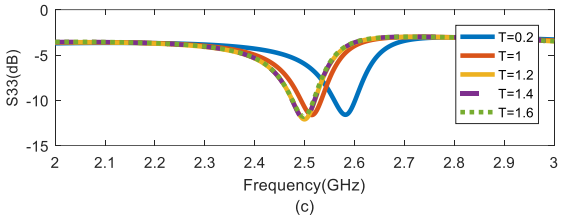

(c)

Fig. 10 (a) Measurement setup for output s-parameters (b) Measured transmission and reflection coefficients (c) The effects of samples' thicknesses on S33.

Comparison of the performance of the proposed sensor and the similar permittivity sensors are presented in TABLE V.

TABLE V
PERFORMANCE COMPARISON OF PROPOSED SENSOR WITH SIMILAR SENSORS

Ref.	f_0 (GHz)	$\frac{\Delta f}{\Delta \epsilon_r}$ (MHz)	S_n (%)	A $(\lambda_g{}^2)$	Material type	Sensor Type
[23]	2.674	63	0.027	0.214	Liquid	IDC in SIW
[16]	2.226	-	0.98	0.038	Liquid	MS in CSRR
[18]	5.65	170	3.25	0.04	Solid	MML.
[20]	2.26	75	3.3	0.01	Solid	IDC in SRR
[14]	2.5	-	0.27	0.07	Liquid	SRR
[29]	2.26	75	3.3	0.01	Solid	IDC-SRR
Proposed	2.895	112	3.9	0.04	Solid	IDC in ML

MS: Meander Slot, MML: Meandered Microstrip line

The normalized sensitivity of the proposed sensor is higher than other sensors. Size of the sensing section are normalized to

guided wavelength. Size comparison shows that the size of sensing part of the proposed sensor is smaller or equal with to similar sensors, except [20] and [29]. However, all of the sensors in TABLE V have one output while the proposed sensor has two identical outputs (two simultaneous channel). This feature help minimizes imperfections in the measurement setup as well as measurement environment. On the other hand, CSRR based planar sensor [30] for complex permittivity measurement shows higher sensitivity than the proposed sensor. However, the applicable range of permittivity seems to be lower ($\Delta\epsilon_r = 0.9$). The dielectric sensor with multiple coupled CSRRs in [31], and the pixelated microwave sensor in [32] demonstrate higher sensitivity as well. However, the normalized sensing area of these sensors (0.1) is larger than that of the proposed sensor.

IV. CONCLUSION

A new T-junction based highly sensitive microwave sensor for permittivity measurement is presented. Interdigital capacitor is used as sensing area in the center of the T-junction. Two outputs of the sensor show the same frequency responses. Therefore, differential mode operation is possible for the proposed structure. Experimental results show that 3.9 % sensitivity has been achieved which is higher than of the reported sensors in the literature. The normalized size of the proposed sensor which include sensing area is comparable with many of the small size sensors in the literature.

The proposed sensor configuration can be further improved for real time differential operation so that any imperfection in measurement environment (spatially distributed temperatures, humidity or other external effects) as well as measurement setup (positioning and other device specific imperfections) could be detected.

REFERENCES

[1] B. D. Wiltshire, T. Zarifi and M. H. Zarifi, "Passive Split Ring Resonator Tag Configuration for RFID-Based Wireless Permittivity Sensing," in IEEE Sensors Journal, vol. 20, no. 4, pp. 1904-1911, 15 Feb.15, 2020, doi: 10.1109/JSEN.2019.2950912.

[2] O. Malyuskin, "Microplastic Detection in Soil and Water Using Resonance Microwave Spectroscopy: A Feasibility Study," in IEEE Sensors Journal, vol. 20, no. 24, pp. 14817-14826, 15 Dec.15, 2020, doi: 10.1109/JSEN.2020.3011311.

[3] P. Mohammadi, A. Mohammadi, S. Demir, and A. Kara, "Compact size, and highly sensitive, microwave sensor for non-invasive measurement of blood glucose level," IEEE Sensors J., vol. 21, no. 14, pp. 16033–16042, Jul. 2021, doi: 10.1109/JSEN.2021.3075576

[4] M. Baghelani, Z. Abbasi and M. Daneshmand, "High-Dynamic-Range Chipless Microwave Resonator-Based Strain Sensor," in IEEE Transactions on Instrumentation and Measurement, vol. 70, pp. 1-7, 2021, Art no. 8003207, doi: 10.1109/TIM.2021.3069375.

[5] C. Wang et al., "High-Accuracy Complex Permittivity Characterization of Solid Materials Using Parallel Interdigital Capacitor- Based Planar Microwave Sensor," in IEEE Sensors Journal, vol. 21, no. 5, pp. 6083-6093, 1 March1, 2021, doi: 10.1109/JSEN.2020.3041014.

[6] R. A. Alahnomi, Z. Zakaria, E. Ruslan, S. R. Ab Rashid and A. A. Mohd Bahar, "High-Q Sensor Based on Symmetrical Split Ring Resonator With Spurlines for Solids Material Detection," in IEEE Sensors Journal, vol. 17, no. 9, pp. 2766-2775, 1 May1, 2017, doi: 10.1109/JSEN.2017.2682266.

[7] A. Aquino, C. G. Juan, B. Potelon and C. Quendo, "Dielectric Permittivity Sensor Based on Planar Open-Loop Resonator," in IEEE Sensors Letters, vol. 5, no. 3, pp. 1-4, March 2021, Art no. 3500204, doi: 10.1109/LSENS.2021.3055544.

[8] L. -V. Herrera-Sepulveda, J. -L. Olvera-Cervantes, A. Corona-Chavez and T. Kaur, "Sensor and Methodology for Determining Dielectric Constant Using Electrically Coupled Resonators," in IEEE Microwave and Wireless Components Letters, vol. 29, no. 9, pp. 626-628, Sept. 2019, doi: 10.1109/LMWC.2019.2928295.

[9] P. Velez, K. Grenier, J. Mata-Contreras, D. Dubuc, and F. Martín, "Highly-sensitive microwave sensors based on open complementary split ring resonators (OCSRRs) for dielectric characterization and solute concentration measurement in liquids," IEEE Access, vol. 6, pp. 48324–48338, 2018.

[10] H. Gan et al., "A CSRR-Loaded Planar Sensor for Simultaneously Measuring Permittivity and Permeability," in IEEE Microwave and Wireless Components Letters, vol. 30, no. 2, pp. 219-221, Feb. 2020, doi: 10.1109/LMWC.2019.2957657.

[11] P. Mohammadi, H. Teimouri, A. Mohammadi, S. Demir and A. Kara, "Dual Band, Miniaturized Permittivity Measurement Sensor With Negative-Order SIW Resonator," in IEEE Sensors Journal, vol. 21, no. 20, pp. 22695-22702, 15 Oct.15, 2021, doi: 10.1109/JSEN.2021.3110611

[12] A. Ebrahimi, J. Scott, and K. Ghorbani, "Ultrahigh-sensitivity microwave sensor for microfluidic complex permittivity measurement," IEEE Trans. Microw. Theory Techn., vol. 67, no. 10, pp. 4269–4277, Oct. 2019.

[13] A. Ebrahimi, W. Withayachumnankul, S. F. Al-Sarawi, and D. Abbott, "Dual-mode behavior of the complementary electric-LC resonators loaded on transmission line: Analysis and applications," J. Appl. Phys., vol. 116, no. 8, 2014, Art. no. 083705.

[14] M. Abdolrazzaghi, M. Daneshmand, and A. K. Iyer, "Strongly enhanced sensitivity in planar microwave sensors based on metamaterial coupling," IEEE Trans. Microw. Theory Techn., vol. 66, no. 4, pp. 1843–1855, Apr. 2018, doi: 10.1109/TMTT.2018.2791942.

[15] A. Ebrahimi et al., "Highly Sensitive Phase-Variation Dielectric Constant Sensor Based on a Capacitively-Loaded Slow-Wave Transmission Line," in IEEE Transactions on Circuits and Systems I: Regular Papers, vol. 68, no. 7, pp. 2787-2799, July 2021, doi: 10.1109/TCSI.2021.3074570.

[16] L. -C. Fan, W. -S. Zhao, D. -W. Wang, Q. Liu, S. Chen and G. Wang, "An Ultrahigh Sensitivity Microwave Sensor for Microfluidic Applications," in IEEE Microwave and Wireless Components Letters, vol. 30, no. 12, pp. 1201-1204, Dec. 2020, doi: 10.1109/LMWC.2020.3029060.

[17] J. Muñoz-Enano, P. Vélez, M. Gil Barba and F. Martín, "An Analytical Method to Implement High-Sensitivity Transmission Line Differential Sensors for Dielectric Constant Measurements," in IEEE Sensors Journal, vol. 20, no. 1, pp. 178-184, 1 Jan.1, 2020, doi: 10.1109/JSEN.2019.2941050.

[18] S. Kiani, P. Rezaei, M. Navaei and M. S. Abrishamian, "Microwave Sensor for Detection of Solid Material Permittivity in Single/Multilayer Samples With High Quality Factor," in IEEE Sensors Journal, vol. 18, no. 24, pp. 9971-9977, 15 Dec.15, 2018, doi: 10.1109/JSEN.2018.2873544.

[19] N. Jankovic and V. Radonic, "A Microwave Microfluidic Sensor Based on a Dual-Mode Resonator for Dual-Sensing Applications," Sensors, vol. 17, no. 12, p. 2713, Nov. 2017.

[20] K. T. Muhammed Shafi, A. K. Jha and M. J. Akhtar, "Improved Planar Resonant RF Sensor for Retrieval of Permittivity and Permeability of Materials," in IEEE Sensors Journal, vol. 17, no. 17, pp. 5479-5486, 1 Sept.1, 2017, doi: 10.1109/JSEN.2017.2724942.

[21] T. Chretiennot, D. Dubuc, and K. Grenier, "Microwave-Based Microfluidic Sensor for Non-Destructive and Quantitative Glucose Monitoring in Aqueous Solution," Sensors, vol. 16, no. 10, p. 1733, Oct. 2016.

[22] T. Chretiennot, D. Dubuc and K. Grenier, "A Microwave and Microfluidic Planar Resonator for Efficient and Accurate Complex Permittivity Characterization of Aqueous Solutions," in IEEE Transactions on Microwave Theory and Techniques, vol. 61, no. 2, pp. 972-978, Feb. 2013, doi: 10.1109/TMTT.2012.2231877.

[23] H. Lobato-Morales, J. H. Choi, H. Lee and J. L. Medina-Monroy, "Compact Dielectric-Permittivity Sensors of Liquid Samples Based on Substrate-Integrated-Waveguide With Negative-Order-Resonance," in IEEE Sensors Journal, vol. 19, no. 19, pp. 8694-8699, 1 Oct.1, 2019, doi: 10.1109/JSEN.2019.2922137.

[24] G. Gugliandolo, K. Naishadham, G. Neri, V. C. Fernicola and N. Donato, "A Novel Sensor-Integrated Aperture Coupled Microwave Patch Resonator for Humidity Detection," in IEEE Transactions on Instrumentation and Measurement, vol. 70, pp. 1-11, 2021, Art no. 9506611, doi: 10.1109/TIM.2021.3062191.

[25] S. Harnsoongnoen, "Metamaterial-Inspired Microwave Sensor for Detecting the Concentration of Mixed Phosphate and Nitrate in Water," in IEEE Transactions on Instrumentation and Measurement, vol. 70, pp. 1-6, 2021, Art no. 9509906, doi: 10.1109/TIM.2021.3086901.

[26] D. M. Pozar, Microwave Engineering, 3rd ed. Hoboken, NJ, USA: Wiley,2005
[27] E. Pettenpaul, H. Kapusta, A. Weisgerber, H. Mampe, J. Luginsland and I. Wolff, "CAD models of lumped elements on GaAs up to 18 GHz," in IEEE Transactions on Microwave Theory and Techniques, vol. 36, no. 2, pp. 294-304, Feb. 1988, doi: 10.1109/22.3518.
[28] Peter A. Rizzi, Microwave Engineering, Englewood Cliffs, NJ, USA: Passive Circuits, Prentice-Hall International, 1988
[29] K. T. Muhammed Shafi, A. K. Jha and M. J. Akhtar, "Improved Planar Resonant RF Sensor for Retrieval of Permittivity and Permeability of Materials," in IEEE Sensors Journal, vol. 17, no. 17, pp. 5479-5486, 1 Sept.1, 2017, doi: 10.1109/JSEN.2017.2724942.
[30] M. A. H. Ansari, A. K. Jha and M. J. Akhtar, "Design and Application of the CSRR-Based Planar Sensor for Noninvasive Measurement of Complex Permittivity," in IEEE Sensors Journal, vol. 15, no. 12, pp. 7181-7189, Dec. 2015, doi: 10.1109/JSEN.2015.2469683.
[31] A. M. Albishi, M. K. E. Badawe, V. Nayyeri and O. M. Ramahi, "Enhancing the Sensitivity of Dielectric Sensors With Multiple Coupled Complementary Split-Ring Resonators," in IEEE Transactions on Microwave Theory and Techniques, vol. 68, no. 10, pp. 4340-4347, Oct. 2020, doi: 10.1109/TMTT.2020.3002996.
[32] Saadat-Safa, M., Nayyeri, V., Ghadimi, A. et al. A Pixelated Microwave Near-Field Sensor for Precise Characterization of Dielectric Materials. Sci Rep 9, 13310 (2019). https://doi.org/10.1038/s41598-019-49767-w

Pejman Mohammadi, received Ph.D. degree in Electrical Engineering from the Middle East Technical University Turkey. Since 2001, he has been with the Department of Electrical Engineering, Islamic Azad University of Urmia, Iran where he is currently Associate Professor. He is also member of Microwave and Antenna Research Center, Urmia Branch, Islamic Azad University, Urmia, Iran. His research interests include microwave component SIW, microwave sensors, microstrip antennas, small antennas for wireless communications, and reconfigurable structures.

Ali Mohammadi, received PhD degree in Electrical Engineering from the University of Newcastle Australia (2014). He conducted post-doctoral research at Monash University and University of Oxford. He is a lecturer (Assistant Professor) at the Department of Electronics and Electrical Engineering, University of Bath, UK. His research interests include microelectromechanical (MEM) devices and microelectronic circuits with applications in micro-energy harvesting and high precision sensing. Dr Mohammadi received MEMS Design Awards form Europractice completions in 2018 and 2020.

Ali Kara received Ph.D. degree from Hacettepe University in 2002. He was with Polytechnic University (ECE), Brooklyn, from 1999 to 2000,

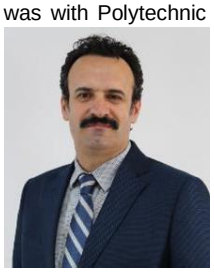

where he conducted theoretical and experimental research. He joined the Department of Electrical and Electronics Engineering of Atilim University, in 2000 and worked until 2021, where he held various positions ranging from lecturer to full professor levels. As of April 2021, he joined the Department of Electrical and Electronics Engineering, Gazi University. He has published extensively in Electromagnetics, Antennas and Propagation as well as Engineering Education. He has four patents, and has led several national and international projects.